Changes in climate and vegetation of central Guizhou in southwest China since the last glacial reflected by stalagmite records from Yelang Cave

Min Zhao [a,b], Hong-Chun Li [b,*], Zai-Hua Liu [a], Horng-Sheng Mii [c], Hai-Long Sun [a], Chuan-Chou Shen [b,d], Su-Chen Kang [b]

[a] State Key Laboratory of Environmental Geochemistry, Institute of Geochemistry, Chinese Academy of Sciences, 46 Guanshui Road, Guiyang 550002, China
[b] Department of Geosciences, National Taiwan University, Taipei 10617, Taiwan, ROC
[c] Department of Earth Sciences, National Taiwan Normal University, Taipei 11677, Taiwan, ROC
[d] High-Precision Mass Spectrometry and Environment Change Laboratory (HISPEC), Department of Geosciences, National Taiwan University, Taipei 10617, Taiwan, ROC

ABSTRACT

Two stalagmites (6-cm and 18-cm long) from Yelang Cave (26°2′28″N, 105°44′11″E) in central Guizhou of China have been dated by ICP-MS [230]Th/U, ^{210}Pb and AMS ^{14}C dating methods. Low U but high Th contents in the young stalagmites were difficult to apply [230]Th/U dating. Instead, AMS ^{14}C dating solved the chronological problem of these stalagmites. Both stalagmites had fast growth rates during Holocene Optimum and the last 600 years, but absent growth between 4 and 8 ka. The $\delta^{18}O$ record of Stalagmite 20120824-13 agrees well with the Dongge $\delta^{18}O$ records on centennial or longer scales, showing dry climates during the Last Glacial Maximum (LGM) and Younger Dryas and wet climates during Holocene Optimum following the solar insolation trend. The summer monsoon strength decreased from 4.12 ka to 1.5 ka, but increased during the Medieval Warm Period to produce wet climates and abundant vegetation in the study area. The $\delta^{18}O$ record during the last 600 years exhibits strongly decadal variations. Twelve light $\delta^{18}O$ excursions on decadal scales during the last 600 years can be identified, agreeing with the local Dry–Wet index record. The Pacific Decadal Oscillation (PDO) strongly affects decadal variability of the moisture budget in the study area, with cold PDO (La Niña condition) in favor of stronger EASM and wet climates. The $\delta^{13}C$ record indicates that natural vegetation in the study area was strongly destroyed by human activity after the reign of Emperor Yong Zheng (AD 1722-1735) of Qing Dynasty. Since then, the karst-desertification in central Guizhou has been strongly developed due to rapidly increased population and land-use.

© 2015 Elsevier Ltd. All rights reserved.

1. Introduction

The East Asian summer monsoon (EASM) affects strongly climatic conditions of East Asia where nearly one-third of the world's population lives in. As a major climatic system, the EASM is not only related to solar insolation and temperature in high latitudes of North Hemisphere (Wang et al., 2001; Wan et al., 2011a), but also interacted/teleconnected with El Niño/Southern Oscillation (ENSO), Intertropical Convergence Zone (ITCZ), North Pacific Subtropical High (NPSH) and Pacific Warm Pool (PWP) (Wang et al., 2006; Wan et al., 2011b; Yin et al., 2014). Studies on variability of the EASM strength and its forcing factors have been

contributed by many precisely dated speleothem records (e.g., Ku and Li, 1998; Li et al., 1998, 2011a,b; Wang et al., 2001, 2005, 2008; Paulsen et al., 2003; Yuan et al., 2004; Hu et al., 2008; Wan et al., 2011a,b; Yin et al., 2014). This is because carbonate cave deposits in the monsoonal regions are assumed to record the intensity of monsoon precipitation as the $\delta^{18}O$ of the carbonate tracks the isotopic signature of precipitation, with a lighter speleothem $\delta^{18}O$ swing indicating stronger summer monsoon and increased rainfall (Li et al., 1998, 2011a,b; Wang et al., 2001, 2005; Yin et al., 2014). On one hand, many speleothem $\delta^{18}O$ records over the eastern China show similarities on orbital scales following the 23-kyr precessional cycles of solar insolation which seems to be a major influencing factor on temperature contrast between land and ocean surface hence the EASM strength (Wang et al., 2001, 2008; Yuan et al., 2004; Wan et al., 2011a; Zhang et al.,

2013). On the other hand, speleothem $\delta^{18}O$ records on interannual-to-centennial scales during the late Holocene show significant discrepancies (e.g., Wan et al., 2011b; Chu et al., 2012; Yin et al., 2014). In general, "amount effect" and changes in $\delta^{18}O$ of moisture source and depositional temperature can all become major factors to influence speleothem $\delta^{18}O$. Hence, influence of solar irradiance variation on the EASM strength and the monsoonal rainfall over monsoonal regions is complicated. For instance, a strengthening of the EASM could result in increased summer rainfall in north and south China, but decreased rainfall in low-middle Yangtze River catchment basins (Zhang et al., 2010). The "amount effect" on speleothem $\delta^{18}O$ may not be the same in different cave sites over eastern China under the same monsoonal regimes. Besides solar activity, ocean–atmospheric circulation on annual-to-centennial scales becomes another important factor to affect the EASM strength (Wang et al., 2006; Yin et al., 2014 and references therein). Apparently, factors to influence the monsoonal rain and speleothem $\delta^{18}O$ on short time scales are much more complicated than these on orbital scales.

Zhang et al. (2010), Wan et al. (2011b) and Chu et al. (2012) have demonstrated spatial variations of the monsoonal rain in different regions of eastern China with modern meteorological observations, historic records and speleothem $\delta^{18}O$ records. On annual to decadal scales, it is clear that a strong summer monsoon can cause wet condition in a region but dry condition in another region in the eastern China, and no simple correlations between EASM intensity and precipitation or temperature. For these reasons, no single speleothem $\delta^{18}O$ record can represent variation of monsoonal precipitation of the entire eastern China (Yin et al., 2014). Therefore, in order to understand paleomonsoon activity and monsoonal climate, more speleothem $\delta^{18}O$ records especially high-resolution, well-dated records of the late Holocene distributed over the monsoonal regions are needed.

Although stalagmite $\delta^{18}O$ records in eastern China have been used as a proxy of summer monsoonal variability, interpretation of the $\delta^{18}O$ in terms of wetness is still under debating as the "amount effect" may not be the major influencing factor. For instance, changes in atmospheric circulation which lead to moisture source change could affect $\delta^{18}O$ of precipitation (Pausata et al., 2011). Since 1950, the EASM strength had a decreasing trend, but the summer rainfall in central China increased. The summer/spring rainfall ratio changed from <1 to >1 after 1950 in Lianhua Cave area, which dominated the stalagmite $\delta^{18}O$ variation on such a time scale (Yin et al., 2014). For this reason, other proxies for climatic conditions in speleothem records are needed. Up-to-date, stalagmite $\delta^{13}C$ is the most common candidate.

As the main source of dissolve inorganic carbon (DIC) in dripping water which is the parent solution for stalagmite formation comes from soil CO_2 and bedrock carbonate dissolution, stalagmite $\delta^{13}C$ registers mainly changes in $\delta^{13}C$ of soil CO_2, portion of CO_2 from bedrock dissolution, and carbon isotopic fractionations caused by degassing, precipitation and dissolution in a cave system. Fairchild et al. (2006) and Li et al. (2012) reviewed factors that influence $\delta^{13}C$ of stalagmite including (1) variation of vegetation (both abundance and C3/C4 plant ratio) or bio-mass above the cave, (2) seasonal change of CO_2-$\delta^{13}C$ in soil, (3) fracture of epikarst zone and difference of latticework in vadose zone (open/close system), (4) residence time of seepage water, (5) dissolution of bedrock, (6) prior precipitation of calcite in vadose zone, and (7) CO_2 degassing of drip water. For the above factors, factors (1) and (2) are related to the biological activity in the overlying soil above a cave and strongly controlled by vegetation change and climatic conditions. On decadal or longer time scales, more abundant vegetation coverage and/or higher C3/C4 ratio under wet climatic conditions produce lighter $\delta^{13}C$ in stalagmites, and vice versa (Ku and Li, 1998; Paulsen et al., 2003). Factors (3)–(6) are related to

hydro-chemical process in the vadose zone and affected by climatic conditions except factor (3). In general, drier condition leads to increase in the residence time of seepage water, the contribution of dissolved bedrock carbonate and prior precipitation of calcite in vadose zone, which in turn result in heavier $\delta^{13}C$ in stalagmites (Fairchild et al., 2006). Therefore, factors (1) to (6) can be considered having similar effects: i.e., a light $\delta^{13}C$ shift in stalagmite under wet climatic conditions, and a heavy $\delta^{13}C$ swing under dry conditions on decadal or longer time scales. Factor (7) is influenced by dripping rate and pCO_2 of cave air. The later one is related to ventilation, temperature and relative humidity of the cave. Stronger CO_2 degassing of drip water under slower dripping rate/stronger ventilation/warmer temperature/low relative humidity will cause heavier $\delta^{13}C$ of calcite deposit in stalagmites (Oster et al., 2010, 2012). Unlike stalagmite $\delta^{18}O$, stalagmite $\delta^{13}C$ is strongly dripping site dependent due to heterogeneity of the DIC-$\delta^{13}C$ in drip water inside a cave (Baker et al., 1997). For some monitoring studies, scientists even found that DIC-$\delta^{13}C$ or $\delta^{13}C$ of speleothem could not remain consistent for the studying periods at the same site of a cave (e.g., Linge et al., 2001). This is the reason why stalagmite $\delta^{13}C$ record is not used as commonly as stalagmite $\delta^{18}O$ record for paleoclimate reconstruction. However, previous studies have published stalagmite $\delta^{13}C$ records and demonstrated that a stalagmite $\delta^{13}C$ record may be used for reconstruction of paleoclimate and paleoenvironment when changes in vegetation and climatic conditions became major factors to control the $\delta^{13}C$ value (e.g., Dorale et al., 1992; Bar-Matthews et al., 1996; Ku and Li, 1998; Genty et al., 2003, 2006, 2010; Paulsen et al., 2003; Zhu et al., 2006; Cosford et al., 2009; Fleitmann et al., 2009; Zhang et al., 2004, 2009; Kuo et al., 2011; Li et al., 2011a,b; Oster et al., 2012; Kotlia et al., 2012; Denniston et al., 2013). These previous studies might indicate that the factors (3)–(7) had relatively weak influence on the $\delta^{13}C$ records on decadal and longer time scales. Recently, more and more cave monitoring studies have shown that speleothem $\delta^{13}C$ records may be used for paleoclimatic and paleoenvironmental reconstructions (Li et al., 2011a,b, 2012; Oster et al., 2010, 2012).

Guizhou Province containing more than 5000 caves is located in the center of the well-known karst regions of South China, and nearly 3/4 of its exposed land is composed of carbonate rocks. However, except stalagmite $\delta^{18}O$ records from Dongge Cave (Yuan et al., 2004; Dykoski et al., 2005; Wang et al., 2005), Yamen Cave (Yang et al., 2010) and Jinshi Cave (Wan et al., 2011a) which are all located in the southeast corner of Guizhou, few speleothem records exist in this abundant cave region. Part of the reason is due to poor quality of $^{230}Th/U$ dating on the stalagmites from central Guizhou because of very low uranium content especially for young stalagmites (Kuo et al., 2011). Recently, we have found that Accelerate Mass Spectrometry (AMS) ^{14}C dating on low U but high Th (detritus) contents is feasible. In this paper, we will present the $\delta^{18}O$ and $\delta^{13}C$ records of two stalagmites from Yelang Cave that is located in central Guizhou. These AMS ^{14}C well-dated stalagmites provide not only the monsoonal climate change but also vegetation variation under climate changes and human impacts in the studying area since last glaciation.

2. Cave site and local climate condition

Yelang Cave (26°2′28.00″N, 105°44′10.93″E) is located in Huangguoshu Township of Anshun City in the central Guizhou where is on the eastern edge of the Yunnan–Guizhou Plateau (Fig. 1). The cave is currently 3 km long with about 1.5 km of groundwater river path. With a hilly topography of karst landscape at an elevation of 1285 m, the region has an annual mean temperature of 15.4 °C and precipitation of 1300 mm based on the
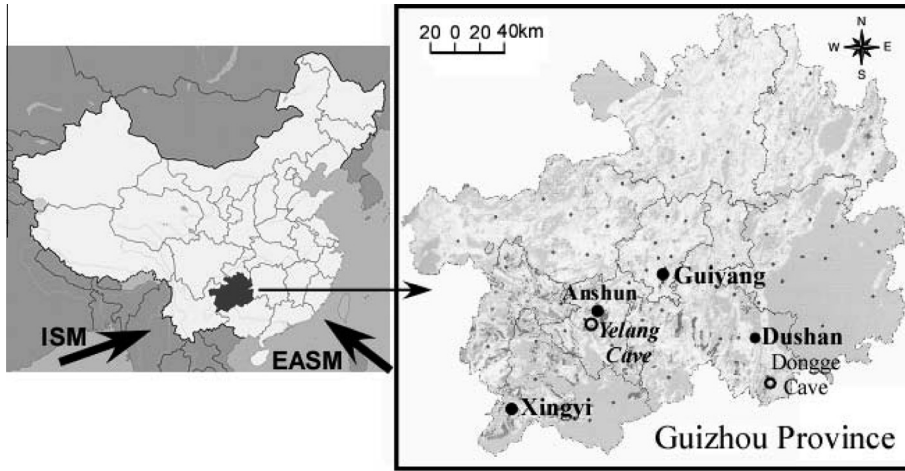
Fig. 1. The location map of study area. Left map shows the location of Guizhou in China. ISM and EASM denote Indian summer monsoon and East Asian summer monsoon, respectively. In the Guizhou map (right), the locations of Yelang Cave (this study), Zhijin Cave (Kuo et al., 2011) and Dongge Cave (Yuan et al., 2004 and Wang et al., 2005) are shown. Locations of four cities where the meteorological records were used are also marked.

meteorological records from 1951 to 2012. Over 75% of the annual rainfall occurs from May to September (Fig. 2), under the influence of EASM. The vegetation around the cave site is dominated by shrub, while the hill in which the cave formed is covered by plants on one side, but is bared with some grasses on the other side. In June of 2013, the measured relative humidity and mean temperature in the cave were ~95% and 17 °C, respectively, and the $\delta^{18}O$ value of the dripping water was −9.04‰ (SMOW). Fig. 3 shows the annual rainfall and mean air temperature variation in four cities of Guizhou from 1951 to 2012. Annual air temperature in Anshun is the lowest among the four cities due to relatively high

elevation and latitude. The rainfall comparison of the four cities appears that four cities have similar variation trends in most years, but opposite trends between south cities (Xingyi and Dushan) and north cities (Anshun and Guiyang), e.g., during 1969–71, 86–88 and 93–94 (Fig. 3). It seems that the rainfall variation in the studying area is more close to that of Western North Pacific Monsoon index (Fig. 3). In order to compare the rainfall variation with other climatic proxies, we use Guiyang rainfall record which goes back to 1920. In Fig. 5, all records are 5-year running average, so that one
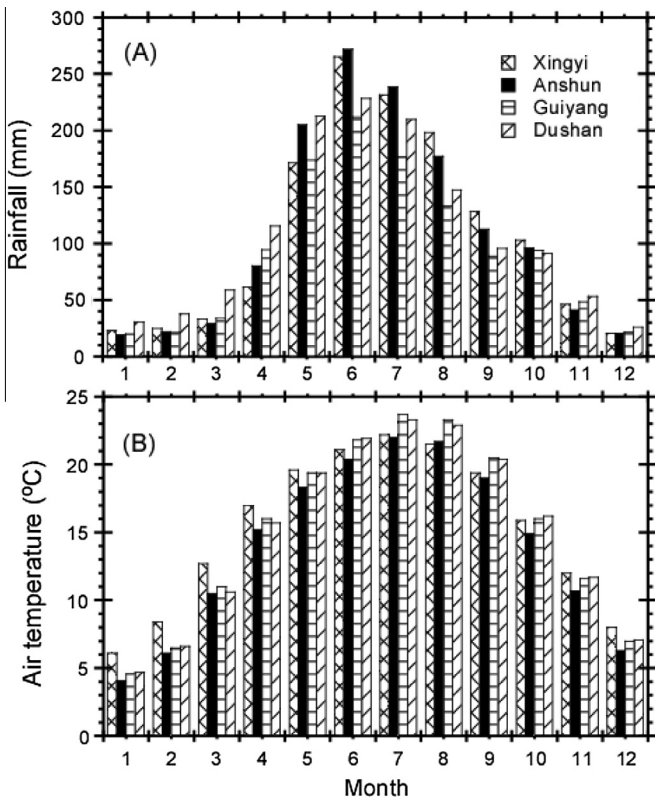

Fig. 2. Monthly rainfall and air temperature of the studying area recorded in four meteorological stations shown in Fig. 1. The monthly averages were calculated from the weather records of 1951–2012. (Data from http://cdc.cma.gov.cn).
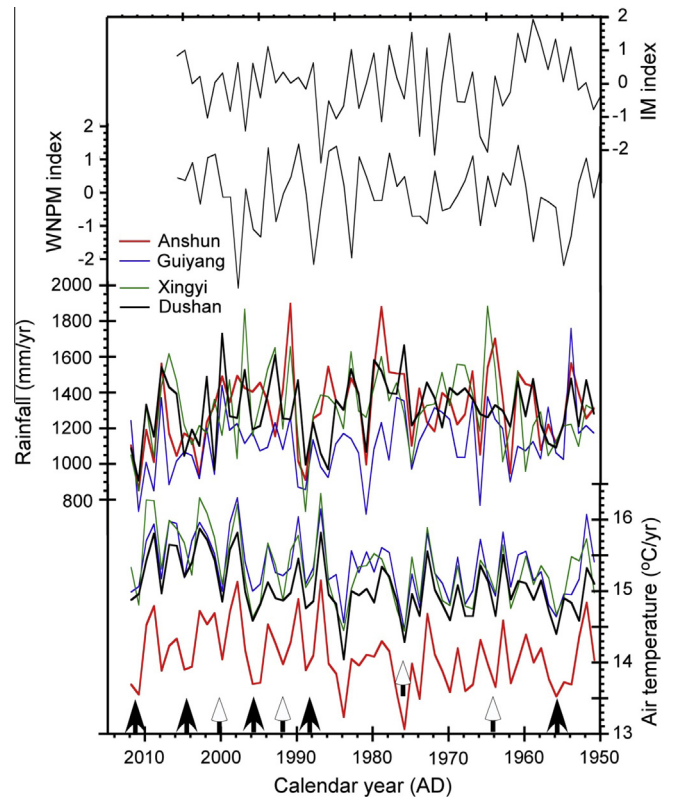

Fig. 3. Comparisons of Indian monsoon index (IM index) and Western North Pacific monsoon index (WNPM index) with annual rainfall and mean temperature variations recorded in the four meteorological stations from 1950 to 2012 (Data from http://cdc.cma.gov.cn). The solid arrows denote cold temperature with low rainfall, whereas the open arrows refer cold temperature with high rainfall.

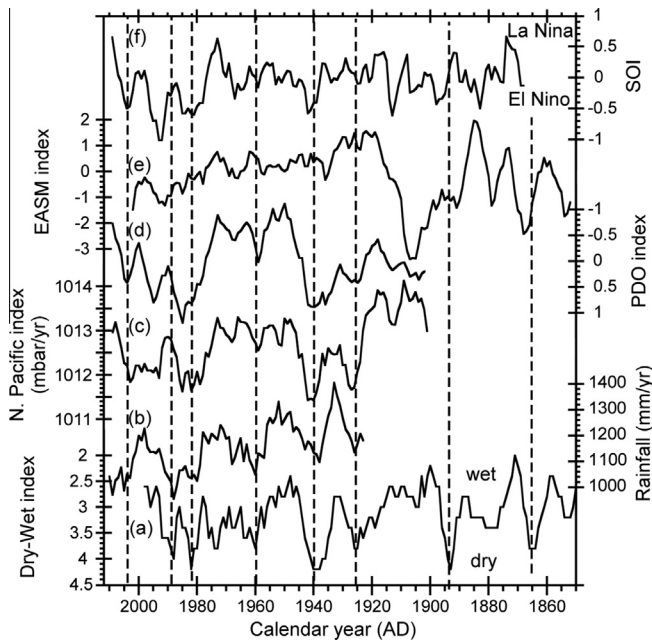**Fig. 4.** Comparisons of (a) Dry–Wet index of Guiyang (CAM, 1981; Zhang et al., 2003), (b) rainfall record of Guiyang (Data from http://cdc.cma.gov.cn), (c) North Pacific index (Data is from NCAR/CGD at http://climatedataguide.ucar.edu), (d) PDO index (Mantua et al., 1997), (e) EASM index (IPCC, 2007), and (f) SOI (Data is from CRU via the page http://www.cru.uea.ac.uk/cru/data/soi/. Allan et al., 1991). (See text for discussion.).

can see general trend comparisons. The Dry–Wet index reconstructed from historic documents in Guiyang extended back to AD 1470 (CAM, 1981; Zhang et al., 2003) agrees well with the instrumentally recorded rainfall record. The comparisons in Fig. 4 indicate that rainfall in the studying area has strong relationship with Pacific Decadal Oscillation (PDO) and North Pacific index, but no clear correlations with EASM index and Southern Oscillation Index (SOI) (Fig. 4). These comparisons will allow us to discuss forcing factors later.

3. Sampling and analytical method

Stalagmites 20120824-11 and 20120824-13 used in this study were collected in an actively developing chamber about 1500 m away from the entrance of Yelang cave. Both stalagmites were alive during the collection with active water dripping on the surface. Stalagmite 20120824-11 is 60 mm in height (Fig. 5). The calcite Stalagmite 20120824-13 is about 180 mm long (Fig. 6). Splitting the stalagmites along the growth axis, their translucent sections have clearly identifiable laminations and growth hiatuses. In Stalagmite 20120824-11, an apparent growth hiatus exists at 18 mm depth. Stalagmite 20120824-13 appears three obvious growth hiatuses at depths of 52, 122 and 130 mm, respectively (Fig. 6).

Powder samples were drilled from split section for ^{230}Th/U dating, Accelerate Mass Spectrometer (AMS) ^{14}C dating, and stable isotope analysis for both 20120824-11 and 20120824-13, but ^{210}Pb dating only for 20120824-13. A total of 14 ^{210}Pb dating samples were taken from the top 30 mm with 2 mm intervals in 20120824-13. ^{210}Pb was analyzed via ^{210}Po alpha-counting method, using a ^{209}Po spike (Li et al., 1996; Kuo et al., 2011). About 0.2 g of each powder sample with ^{209}Po spike was dissolved by 4 N HNO$_3$. Concentrated HNO$_3$ and HCl were used to dissolve impurities. The solution was evaporated to dryness. Then, using 1.0 N HCl to dissolve the residues. The solution was transferred into a 50-ml centrifuge tube. Adding powders of ascorbic acid into the solution little by little until the solution becomes clear, so that all dissolved Fe ions can be combined with the ascorbic acid. Put a silver disc (0.8 cm in diameter) into the solution, and place the tube in a temperature controlled water bath. Polonium was self-plated from the solution onto the silver diskette under 80 °C. The silver diskette was then counted for ^{209}Po and ^{210}Po in an ORTEC 576A alpha spectrometric system. The results are given in Table 1 and plotted in Fig. 7.

In this study, seven samples for AMS ^{14}C dating (ellipse spots in Fig. 5) and 6 samples for ICP-MS ^{230}Th/U dating (black squares) were taken from Stalagmite 20120824-11 (Fig. 5), and samples from 22 horizons for AMS ^{14}C dating and 11 samples for ICP-MS ^{230}Th/U dating were taken from Stalagmite 20120824-13 (Fig. 6). For AMS ^{14}C dating on the upper 30 mm in Stalagmite 20120824-13, we took second batch of five samples (−17 to −21) to check the results. The ^{230}Th/U dating was performed in the High-precision Mass Spectrometry and Environment Change Laboratory (HISPEC) at the National Taiwan University. All chemical procedures followed the method described in Shen et al. (2002, 2003). The instrument for Th and U isotopic analyses is a Finnigan Neptune multi-collector inductively coupled plasma mass spectrometer (MC-ICP-MS) (Shen et al., 2012). Although the dating
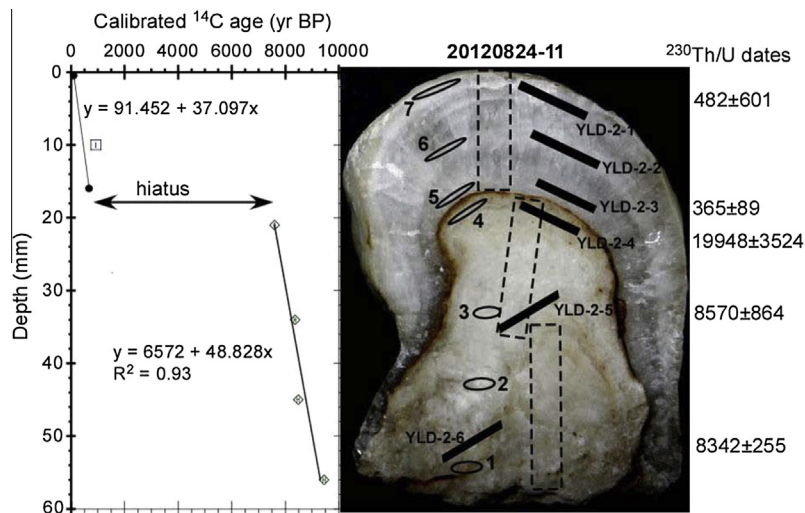

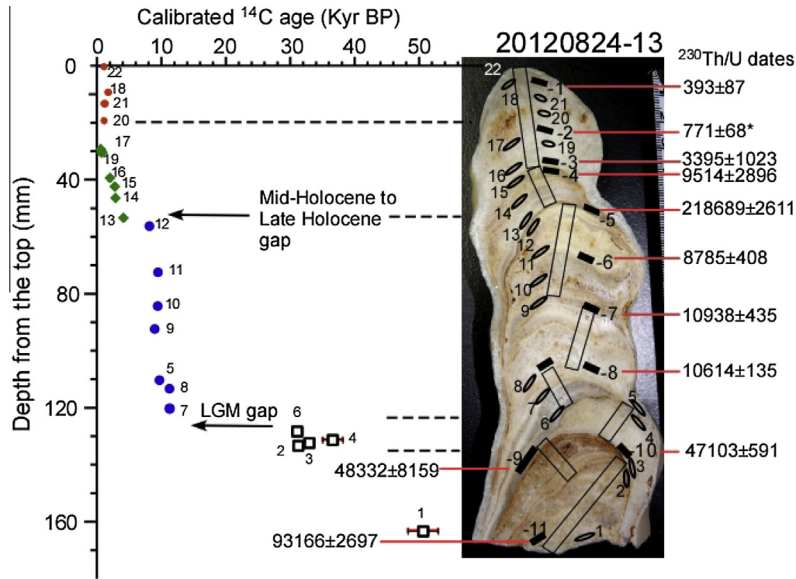**Fig. 5.** Picture of Stalagmite 20120824-11 with ^{230}Th/U dates and AMS ^{14}C dates.

Fig. 6. Picture of Stalagmite 20120824-13 with [230]Th/U dates and AMS ^{14}C dates.

Table 1
[210]Pb in stalagmite 20120824-13 from Yelang cave.

| Sample	Depth (mm)	Measured [210]Pb (dpm/g)	Excess [210]Pb (dpm/g)
20120824-13-1	1 ± 1	0.56 ± 0.08	0.48 ± 0.09
20120824-13-2	3 ± 1	0.15 ± 0.05	0.07 ± 0.07
20120824-13-3	5 ± 1	0.44 ± 0.07	0.36 ± 0.09
20120824-13-4	7 ± 1	0.31 ± 0.05	0.23 ± 0.07
20120824-13-5	9 ± 1	0.20 ± 0.07	0.12 ± 0.09
20120824-13-6	11 ± 1	0.17 ± 0.05	0.09 ± 0.07
20120824-13-7	13 ± 1	0.09 ± 0.03	0.01 ± 0.06
20120824-13-8	15 ± 1	0.16 ± 0.05	
20120824-13-9	17 ± 1	0.13 ± 0.05	
20120824-13-10	19 ± 1	0.13 ± 0.09	
20120824-13-11	21 ± 1	0.08 ± 0.06	
20120824-13-12	23 ± 1	0.26 ± 0.08	
20120824-13-13	25 ± 1	0.14 ± 0.06	
20120824-13-14	27 ± 1	0.33 ± 0.10	
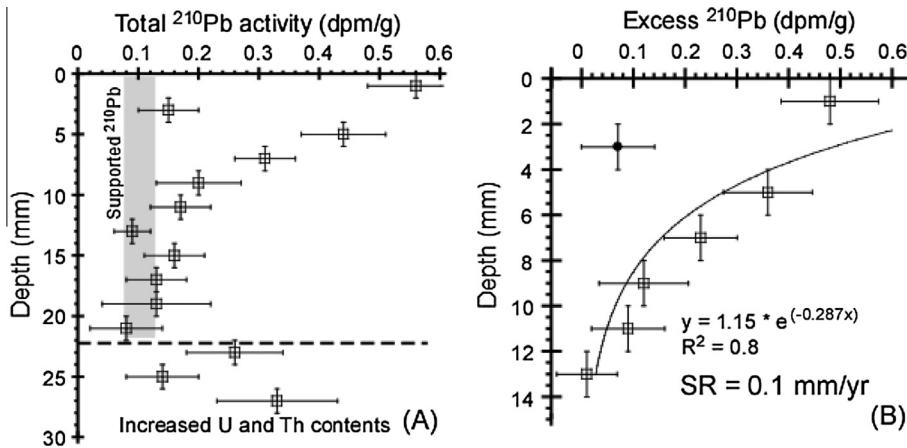
Fig. 7. [210]Pb dating profiles of Stalagmite 20120824-13. (A) Total ^{210}Pb profile. (B) Excess ^{210}Pb profile. The data point at 3 mm depth in (B) is not included in the fitting. [210]Pb in the upper 14 mm exhibits an exponential decrease due to radioactive of ^{210}Pb, which indicates an average of growth rate of ~0.1 mm/year in the top 14 mm of this stalagmite.

technique and facility of the HISPEC Lab are state-of-art and well-known world class, the analytical precision of these samples are very poor mainly due to very low U contents and relatively high Th detritus. All ^{230}Th/U dating results are listed in Table 2.

For AMS ^{14}C dating, the samples need to be converted to graphite. Stalagmite sample dissolution is carried out in a specially designed finger flask that contains a side arm for phosphoric acid reservoir. About 10 mg of the stalagmite powders wrapped in a tin cup were placed into the reaction vessel of the flask and 1 ml of 100% H_3PO_4 was added to the side arm with a clean Pasteur pipette. The flask was connected to a vacuum line for evacuating the air. After the vacuum reached 10^{-3} mbar, the reaction vessel was sealed and removed from the line. Tilting the reaction vessel to allow the H_3PO_4 in the side arm to spill out and react with the stalagmite sample. The reaction vessel was then connected with the vacuum line again. The produced gases were passing through a water trap under $-60\,°C$, and frozen into a glass tube by liquid nitrogen. The purified CO_2 was measured its volume and then sealed into the glass tube. The tube that contains purified CO_2 sample was placed on the graphitization line under vacuum of 10^{-3} mbar. While about 400 mg Zn under $450\,°C$ presented for catalysis, the CO_2 was reduced to graphite with Fe (Fe:C = 3.5:1) under $550\,°C$ for 6–8 h. Graphite samples were pressed into targets and measured for their ^{14}C/^{12}C and ^{13}C/^{12}C ratios with oxalic acid standards (OXII, 4900C) at the Accelerate Mass Spectrometer Radiocarbon Dating Laboratory of the National Taiwan University (NTUAMS Lab). A 1.0MV Tandetron Model 4110 BO-AMS made by High Voltage Engineering Europa B.V. (HVEE) is equipped in the NTUAMS Lab. The maximum number of targets for each wheel is 50. For each batch of samples, at least 3 OXII standard and 3 background samples are processed and measured with the samples. We measure C^{3+} to avoid Lithium (Li_2^+) interference. Every target is measured three cycles, and each cycle contains 100 blocks which last 50 min. The AMS ^{14}C counting statistical error for OXII is generally less than 5‰. The background level of the AMS ^{14}C dating was measured by using NTUB which is pure calcite of an upper Devonian limestone from Guilin, China. Radiocarbon ages are determined with a half-life of 5568 years and corrected the isotopic fractionation with measured ^{13}C/^{12}C ratio by the AMS. The conventional ^{14}C ages are converted to calibrated calendar ages (year BP = years before AD 1950) using CalPal Online Radiocarbon Calibration of ^{14}C (http://www.calpal-online.de/) and CALIB 7.0 (http://calib.qub.ac.uk/calib/) (Stuiver and Reimer, 1986, 1993). All AMS ^{14}C dates are listed in Table 3.

For δ^{18}O and δ^{13}C analyses, a total of 1283 subsamples were drilled from 20120824-13 at an interval of 0.1 mm from top to 51 mm and an interval of 0.2 mm from 51 mm to the bottom of 175 mm (rectangles in Fig. 6). A total of 592 subsamples were taken along the growth axis of 20120824-11. However, after the dating work of the stalagmites was finished, we decided to measure 440 subsamples of 20120824-13 and 50 subsamples of 20120824-11 for δ^{18}O and δ^{13}C analyses. Thus, the stable isotope records for the upper 37-mm part has high-resolution at 0.1 mm interval, and the resolutions for the rest parts are lower. Samples were analyzed in two stable isotope laboratories: one is in the Department of Geosciences at the National Taiwan University (NTU) which has a Finnigan MAT-253 isotopic ratio mass spectrometer (IRMS) equipped with a Kiel-III Carbonate Device; and the other is in the Department of Earth Sciences at the National Taiwan Normal University (NTNU) containing a Micromass IsoPrime IRMS equipped with a Multicarb automatic system. The δ^{18}O and δ^{13}C values reported here are relative to the Vienna PeeDee Belemnite (VPDB) standard at $25\,°C$. The standard deviations of NBS-19 runs are normally 0.08‰ for δ^{18}O and 0.06‰ for δ^{13}C. A working standard, MAB (a pure marble formed in Taroko

Table 2
^{230}Th/U dating results on Stalagmites 20120824-13 (YLD-1-1 to YLD-1-11) and 20120824-11 (YLD-2-1 to YLD-2-6).

Sampl .ID	Depth (mm)	^{238}U ppb[a]	^{232}Th ppt	δ^{234}U meas.[a]	[^{230}Th/^{238}U] activity[c]	[^{230}Th/^{232}Th] ppm[d]	Age Uncorr.	Age Corr.[c,e]	δ^{234}U$_{initial}$ Corr.[b]
YLD-1-1	3 ± 1	22.43 ± 0.05	130 ± 3.9	158 ± 5.0	0.0056 ± 0.0006	15.79 ± 1.72	526 ± 55	393 ± 87	158 ± 5.0
YLD-1-2	27 ± 1	25.03 ± 0.04	981 ± 5.1	179 ± 3.7	0.0083 ± 0.0007	3.50 ± 0.31	771 ± 68	−111 ± 448	179 ± 3.8
YLD-1-3	34 ± 1	27.09 ± 0.07	2418 ± 7.5	187 ± 4.6	0.0574 ± 0.0015	10.60 ± 0.28	5400 ± 150	3395 ± 1023	188 ± 4.7
YLD-1-4	38 ± 1	17.34 ± 0.03	4281 ± 15	196 ± 4.3	0.1550 ± 0.0044	10.35 ± 0.29	15,085 ± 459	9514 ± 2896	201 ± 4.7
YLD-1-5	50 ± 1	60.03 ± 0.10	22 ± 4.9	213 ± 2.7	1.0967 ± 0.0034	49,224 ± 10,857	218,696 ± 2611	218,689 ± 2611	395 ± 5.9
YLD-1-6	70 ± 1	48.56 ± 0.08	1550 ± 7.6	171 ± 2.7	0.0980 ± 0.0019	50.63 ± 0.99	9505 ± 190	8785 ± 408	176 ± 2.8
YLD-1-7	90 ± 1	78.64 ± 0.14	2969 ± 12	221 ± 2.3	0.1252 ± 0.0015	54.66 ± 0.67	11,754 ± 146	10,938 ± 435	228 ± 2.4
YLD-1-8	113 ± 1	53.16 ± 0.10	401 ± 4.5	236 ± 3.3	0.1166 ± 0.0011	255.3 ± 3.70	10,775 ± 109	10,614 ± 135	243 ± 3.4
YLD-1-9	132 ± 1	49.42 ± 0.09	34678 ± 380	298 ± 2.6	0.5810 ± 0.0146	13.65 ± 0.37	63,051 ± 2102	48,332 ± 8159	341 ± 8.2
YLD-1-10	133 ± 1	50.46 ± 0.08	2133 ± 6.6	284 ± 3.0	0.4635 ± 0.0030	180.8 ± 1.28	47,951 ± 414	47,103 ± 591	324 ± 3.4
YLD-1-11	172 ± 1	60.48 ± 0.08	12193 ± 64	222 ± 2.2	0.7385 ± 0.0081	60.40 ± 0.73	97,379 ± 1689	93,166 ± 2697	289 ± 3.6
YLD-2-1	2.5 ± 0.5	30.15 ± 0.05	1609 ± 6.1	197 ± 3.9	0.0182 ± 0.0008	5.61 ± 0.25	1668 ± 75	482 ± 601	197 ± 3.9
YLD-2-3	13 ± 0.5	33.57 ± 0.04	211 ± 4.2	218 ± 2.5	0.0056 ± 0.0006	14.68 ± 1.71	501 ± 58	365 ± 89	218 ± 2.5
YLD-2-4	18 ± 0.5	38.31 ± 0.10	11061 ± 51	159 ± 4.8	0.2528 ± 0.0049	14.44 ± 0.29	26,683 ± 597	19,948 ± 3524	168 ± 5.3
YLD-2-5	35 ± 1.5	35.90 ± 0.08	2558 ± 8.7	126 ± 4.0	0.1012 ± 0.0016	23.42 ± 0.38	10,251 ± 174	8570 ± 864	129 ± 4.1
YLD-2-6	51 ± 1.0	50.20 ± 0.17	1033 ± 4.3	153 ± 5.0	0.0897 ± 0.0009	71.87 ± 0.71	8813 ± 97	8342 ± 255	157 ± 5.1

Chemistry was performed on October 14th, 2013 (Shen et al., 2003), and instrumental analysis on MC-ICP-MS (Shen et al., 2012). Analytical errors are 2σ of the mean.
[a] [^{238}U] = [^{235}U] × 137.818 (±0.65‰) (Hiess et al., 2012); δ^{234}U = ([^{234}U/^{238}U]$_{activity}$ − 1) × 1000.
[b] δ^{234}U$_{initial}$ corrected was calculated based on ^{230}Th age (T), i.e., δ^{234}U$_{initial}$ = δ^{234}U$_{measured}$ $Xe^{\lambda 234 \times T}$, and T is corrected age.
[c] [^{230}Th/^{238}U]$_{activity}$ = 1 − $e^{-\lambda 230T}$ + (δ^{234}U$_{measured}$/1000)[λ_{230}/(λ_{230} − λ_{234})](1 − $e^{-(\lambda 230 - \lambda 234)T}$), where T is the age. Decay constants are 9.1705×10^{-6} yr^{-1} for ^{230}Th, 2.8221×10^{-6} yr^{-1} for ^{234}U (Cheng et al., 2013), and 1.55125×10^{-10} yr^{-1} for ^{238}U (Jaffey et al., 1971).
[d] The degree of detrital ^{230}Th contamination is indicated by the [^{230}Th/^{232}Th] atomic ratio instead of the activity ratio.
[e] Age corrections for samples were calculated using an estimated atomic ^{230}Th/^{232}Th ratio of 4 ± 2 ppm. Those are the values for a material at secular equilibrium, with the crustal ^{232}Th/^{238}U value of 3.8. The errors are arbitrarily assumed to be 50%.

Table 3
AMS dating results on 20120824-13 and 20120824-11.

Lab code	Sample Id	Depth (mm)	pMC (%)	Δ^{14}C (‰)	Age (yr BP)	Calib. age (yr BP)
NTUAMS-873	20120824-13-22	0.1	86.46	−135.39	1169 ± 5	1095 ± 25
NTUAMS-569	20120824-13-18	9	79.88	−201.20	1805 ± 9	1750 ± 30
NTUAMS-871	20120824-13-18	9	79.25	−207.51	1868 ± 12	1830 ± 30
NTUAMS-749	20120824-13-21	13	84.42	−155.77	1360 ± 1	1295 ± 5
NTUAMS-828	20120824-13-21	13	86.25	−137.51	1188 ± 4	1115 ± 30
NTUAMS-748	20120824-13-20	19	87.09	−129.09	1110 ± 1	1015 ± 35
NTUAMS-872	20120824-13-20	19	86.19	−138.11	1194 ± 3	1125 ± 35
NTUAMS-570	20120824-13-17	28	93.43	−65.65	546 ± 4	545 ± 5
NTUAMS-826	20120824-13-17	28	92.66	−73.35	612 ± 1	605 ± 40
NTUAMS-747	20120824-13-19	30	89.96	−100.38	850 ± 1	850 ± 1
NTUAMS-827	20120824-13-19	30	91.89	−81.10	679 ± 2	665 ± 5
NTUAMS-568	20120824-13-16	34	77.40	−226.04	2058 ± 6	2025 ± 20
NTUAMS-567	20120824-13-15	40	72.05	−279.46	2633 ± 10	2760 ± 5
NTUAMS-566	20120824-13-14	46	70.71	−292.86	2784 ± 8	2890 ± 20
NTUAMS-565	20120824-13-13	50	62.73	−372.72	3746 ± 9	4120 ± 25
NTUAMS-564	20120824-13-12	54	44.04	−559.55	7723 ± 36	8505 ± 45
NTUAMS-563	20120824-13-11	68	34.40	−655.98	8572 ± 63	9565 ± 55
NTUAMS-562	20120824-13-10	81	34.81	−651.86	8476 ± 37	9505 ± 25
NTUAMS-561	20120824-13-9	90	36.32	−636.77	8135 ± 26	9070 ± 35
NTUAMS-557	20120824-13-5	112	33.75	−662.52	8726 ± 35	9690 ± 70
NTUAMS-560	20120824-13-8	113	29.01	−709.89	9941 ± 38	11350 ± 30
NTUAMS-559	20120824-13-7	121	29.08	−709.16	9921 ± 42	11330 ± 60
NTUAMS-558	20120824-13-6	131	3.79	−962.05	26280 ± 394	31110 ± 430
NTUAMS-556	20120824-13-4	133	1.87	−981.28	31957 ± 1270	36625 ± 1580
NTUAMS-555	20120824-13-3	134	2.87	−971.34	28534 ± 355	32995 ± 500
NTUAMS-554	20120824-13-2	135	3.65	−963.54	26602 ± 397	31285 ± 440
NTUAMS-553	20120824-13-1	168	0.29	−997.13	47031 ± 1163	50660 ± 2330
NTUAMS-880	20120824-11-7	0.5	98.66	−1.34	109 ± 0.5	110 ± 1
NTUAMS-879	20120824-11-6	10	88.56	−114.43	976 ± 3	925 ± 5
NTUAMS-878	20120824-11-5	16	91.05	−89.51	753 ± 3	685 ± 5
NTUAMS-877	20120824-11-4	21	43.30	−566.98	6723 ± 24	7600 ± 15
NTUAMS-876	20120824-11-3	34	39.12	−608.85	7540 ± 41	8370 ± 30
NTUAMS-875	20120824-11-2	45	38.37	−616.33	7695 ± 35	8485 ± 45
NTUAMS-874	20120824-11-1	56	35.09	−649.08	8412 ± 42	9450 ± 40
NTUAMS-1412	YLD20141122		108.58	85.84		

National Park of Eastern Taiwan ca. 250 million years ago with $\delta^{18}O = -6.9‰$ and $\delta^{13}C = 3.4‰$), was measured after every 5–7 sample measurements to monitor any instrumental drift.

4. Results and discussions

4.1. ^{230}Th dating

Stalagmite 20120824-11 contains very low U (<0.05 ppm) and an apparent growth hiatus at 1.8-cm depth (Fig. 5 and Table 2). The ^{230}Th/U dates show some reversed age sequences with large uncertainties. The upper 1.8-cm of the stalagmite was deposited during the past 400 years, and below the hiatus the stalagmite grew in early Holocene. The calcite stalagmite of 20120824-13 has three obvious growth hiatus at depths of 52, 122 and 130 mm respectively (Fig. 6). All the samples with low U contents (0.017–0.08 ppm) and high Th levels of 20120824-13 have posed a considerable challenge to the ^{230}Th/U dating. The dating results show large error (>5% in general) and some reversed ages. Although an age-depth relationship cannot be obtained using the ^{230}Th/U ages for both stalagmites, the ages still reveal three growth periods of Stalagmite 20120824-13: 40–90 kyr BP (below 130 mm depth), 4–11 kyr BP (50–130 mm) and 400 year BP-present (above 50 mm depth); and two growth periods of Stalagmite 20120824-11: 8000–9000 yr BP and 400–0 yr BP (Table 2). Note that the initial ^{230}Th corrected age of YLD-1-2 is −111 ± 448 a which is not reasonable, perhaps caused by incorrect assumption of using an estimated atomic ^{230}Th/^{232}Th ratio of 4 ± 2 ppm. For this age, we use uncorrected age of 771 ± 68 a.

4.2. ^{210}Pb dating

The ^{210}Pb dating attempts to determine whether the surface of Stalagmite 20120824-13 is modern. As shown in the Table 1 and Fig. 7, ^{210}Pb activity in 20120824-13 is very low due to low U contents. The total ^{210}Pb activity reached relatively constant value between 14 and 21 mm, and slightly increased below 21 mm perhaps due to increased U content (Table 2). Thus, we select the average of four total ^{210}Pb values between 14 and 21 mm as supported ^{210}Pb activity (Fig. 7A). The excess ^{210}Pb activity in each layer is using total ^{210}Pb activity to subtract this average value. The ^{210}Pb activity at 3-mm depth is anomaly low, so that it is excluded in the fitting trend. The fitting of excess ^{210}Pb decay trend yields an average growth rate of 0.1 mm/year (Fig. 7B). The fact that excess ^{210}Pb decay trend in the upper 14 mm of Stalagmite 20120824-13 confirms the surface of the stalagmite is modern and the age of 14-mm depth should be older than 120 year (>five $T_{1/2}$ of ^{210}Pb). If we apply the growth rate of 0.1 mm/year to the upper 30 mm of the stalagmite, the age at the 30 mm depth is about 300 years which is apparently younger than the results of AMS ^{14}C dating and ^{230}Th/U dating. The growth rate given by the ^{210}Pb dating may be overestimated.

4.3. AMS ^{14}C dating

Normally, radiocarbon dating is not considered for stalagmite dating because of dead carbon influence during the carbonate precipitation. However, when ^{230}Th/U dating is not applicable, AMS ^{14}C dating is an alternative choice. It is certain that when seepage

water passes through the limestone bedrock, dissolution of carbonate will bring dead carbon into the solution. Therefore, it is normal to have dead carbon influence when stalagmite forms. Previous studies have estimated dead carbon fraction (DCF) in stalagmites (Beck et al., 2001; Genty et al., 2001; Hoffmann et al., 2010; Oster et al., 2010; Southon et al., 2012). It seems that DCF in ^{14}C age varied in every stalagmite and sometimes changed with time. In some cases, DCF was less than 1% which had little influence on ^{14}C age. This is because when dissolved CO_2 in the seepage water exchange well with atmospheric CO_2 in an open system of carbonate reservoir, the dead carbon influence becomes minimal (Hendy, 1971). For such cases, the ^{14}C ages may be used to reconstruct stalagmite chronology.

The AMS ^{14}C dates of Stalagmites 20120824-11 and -13 are listed in Table 3. One of the samples (YLD20141122) is modern calcite deposited from July 2013 to November 2014. The ^{14}C activity of this sample is higher than that of standard modern carbon with percentage of modern carbon (pMC) being 108.58%, containing significant amount of "nuclear bomb carbon". The AMS ^{14}C dates of Stalagmite 20120824-11 indicate that the upper 1.8-cm has been continuously grown over the past 685 years because no hiatus can be found in this section (Fig. 5). The lower part of Stalagmite 20120824-11 formed in early Holocene between 7600 and 9450 year BP. The AMS ^{14}C dating results of this stalagmite agree with the ^{230}Th/U dating results, but with small uncertainty and better age sequence (Fig. 5). For Stalagmite 20120824-13, the AMS ^{14}C dates from the upper 20 mm part appear significant dead carbon influence because two lower samples (−17 and −19) have younger ^{14}C dates. In order to confirm the results, second sample was taken from the same place for five layers. Although the ages are not exactly the same for the duplicated samples due to sampling uncertainty, the ages are very close each other at the same layer (Table 3). Average values of each pair ages for these five layers were used. The upper 30 mm part of Stalagmite 20120824-13 is 760 yr BP, whereas the ^{230}Th/U dating and ^{210}Pb dating indicate that this part is younger than 770 years. The AMS ^{14}C dates between 30 mm and 51 mm are from 2025 yr BP to 4120 yr BP with good sequences, probably having little dead carbon influence. Below the hiatus at 52 mm, the AMS ^{14}C dates between 54 mm and 121 mm are 8505 yr BP to 11350 yr BP, agreeing with the ^{230}Th/U dates (Fig. 6). Below the Last Glacier Maximum (LGM) gap at 121 mm, four AMS ^{14}C dates between 122 mm and 130 mm concentrate on 31–36 kyr BP, much younger than the two ^{230}Th/U dates of 47–48 Ka. The AMS ^{14}C date at the bottom (168 mm) is ~50 kyr BP, also much younger than the ^{230}Th/U date of 93 Ka. The phenomenon that AMS ^{14}C date is younger than ^{230}Th/U date reflects negligible dead carbon influence in the AMS ^{14}C dates and strong influence of initial ^{230}Th in ^{230}Th/U ages. Using estimated ^{230}Th/^{232}Th ratio of 4 ± 2 ppm for ^{230}Th/U age corrections for samples below 121 mm depth may not be suitable.

4.4. Chronology of 20120824-11 and 20120824-13

From Figs. 5 and 6, we can see that the AMS ^{14}C dating results for Holocene section generally agree with the ^{230}Th/U dating results, but with much less analytical uncertainty and better age sequence. For older than Holocene part, neither AMS ^{14}C nor ^{230}Th/U dating results are able to provide age-depth relationship. Based on the results of ^{210}Pb dating, AMS ^{14}C dating and ^{230}Th/U dating, we can reconstruct the age-depth relationships for the Holocene sections of Stalagmites 20120824-11 (Fig. 5) and 20120824-13 (Fig. 8). Stalagmite 20120824-11 contains two growth periods: over the past 685 yr BP for 0–18 mm and from 9.5 kyr BP to 7.6 kyr BP below 18 mm depth. Linear growth rates of the two periods are 0.027 mm/yr and 0.02 mm/yr, respectively. In Stalagmite 20120824-13, there are six different growth periods:
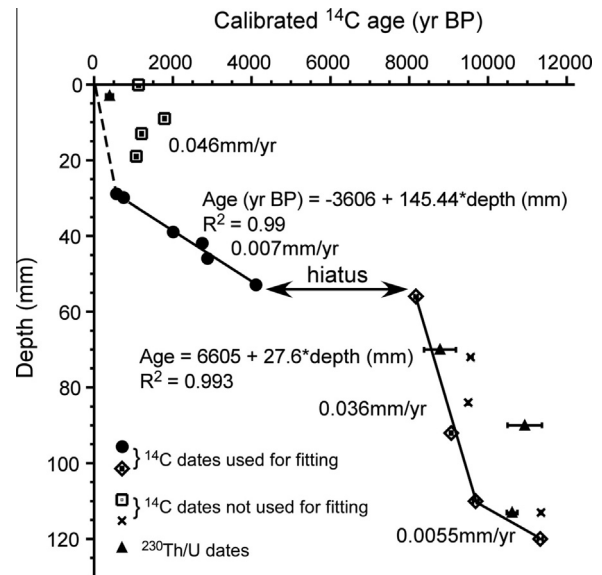

Fig. 8. Reconstructed the Holocene chronology with depth of 20120824-13. The dashed line indicates the extrapolating fitting between the modern surface and the AMS ^{14}C date at 28 mm depth. Due to the dead carbon influence, the AMS ^{14}C dates above 25 mm depth were excluded for chronology reconstruction.

(1) Section below 135 mm (>40 kyr BP) formed during the Marine Oxygen Isotope Stage (MOIS) 3. Calcite deposition in this section appeared dark brown, indicating more impurities from the surface above the cave (Fig. 6). (2) From 135 to 131 mm (around 31 kyr BP) just before the LGM. After the section, a major hiatus occurred at 122 mm depth resulted from cold and dry conditions during the LGM (Fig. 6). (3) From 130 to 112 mm (12–10 kyr BP), the stalagmite grew very slow with a growth rate of 0.0055 mm/yr (Fig. 8). (4) From 112 to 54 mm (10–8.2 kyr BP), the stalagmite grew fast with a growth rate of 0.036 mm/yr, corresponding to warm and humid climates during the Holocene Optimum (HO). At 8.2 kyr BP, a major growth hiatus existed, probably caused by the 8.2 kyr BP cold event. (5) During the mid-Holocene, the stalagmite did not grow. The stalagmite started to grow again after 4.12 kyr BP with a linear growth rate of 0.007 mm/yr until ~600 years ago for the section of 52–28 mm. (6) For the upper 28 mm, the stalagmite grew fast with an average growth rate of 0.046 mm/yr over the past 600 years. We admit that the dating results on the stalagmites from Yelang Cave are not very accurate due to low U contents, relatively high Th contents and dead carbon influence. But, this is the best we could have done. Nevertheless, the reconstructed chronologies may not accurate on decadal time scale, but should be valid at least on centennial scales. With the current chronologies, we shall interpret the δ^{18}O and δ^{13}C records of Stalagmite 20120824-13.

4.5. Comparisons between two isotopic records and with climate records

Before the stable isotope records of Yelang cave are interpreted for climatic and environmental changes, the isotopic equilibrium fractionation should be examined. For this purpose, three approaches are used: (1) using the δ^{18}O of dripping water and cave temperature to calculate the equilibrated calcite δ^{18}O value; (2) comparison of the δ^{18}O records between 20120824-11 and 20120824-13; and (3) comparison of the δ^{18}O records with rainfall record and Dry–wet index record of Guiyang. The δ^{18}O values of cave waters in Yelang cave during 2013–2014 range from −9.21‰ to −8.56‰ (SMOW), with an average δ^{18}O of −9.04‰

(SMOW) for drip water. The annual mean cave temperature in Yelang cave measured in 2013 was 17 °C. We can calculate the calcite δ18O value under isotope equilibrium fractions by the simplified equation (modified from O'Neil et al., 1969; Friedman and O'Neil, 1977):

$$\delta^{18}O_C \text{ (PDB)} = 3.945 - 0.232 \times T \text{ (°C)} + \delta^{18}O_W \text{ (SMOW)}$$

where $\delta^{18}O_c$ is the δ18O of calcite; $\delta^{18}O_W$ is the δ18O of parent water, and T is the equilibrium temperature. The calculated $\delta^{18}O_c$ is −9.03‰ (PDB) under isotopic equilibrium fractionation, close to the δ18O of −9.40‰ in the top of 20120824-13. If warm season temperature is used, the calculated $\delta^{18}O_c$ will be lighter.

Stalagmites 20120824-11 and 20120824-13 grew nearby. Instead of Hendy Test, similarity of the two δ18O records should be the best evidence for validation of the records (Yin et al., 2014 and refs. therein). Fig. 9 shows the comparison of the two records which have independent age controls. Note that the chronologies of the comparison part in both stalagmites have only two age control points, so that the linear growth rates may have age uncertainties. Although the large uncertainties in the chronology of the records do not allow us to match the two records very well, the major features in both δ18O records are comparable (letters in Fig. 9). The variation trends of both δ13C records are also similar. A depleting trend occurred around late 20 century in both δ13C records. If a higher growth rate as suggested by the 210Pb dating is used, the comparison may be better. Nevertheless, using the current chronologies, the comparisons are still feasible and the two stalagmite records support each other.

As mentioned before, although multiple factors such as temperature and changes in moisture source and its δ18O can affect the δ18O of a stalagmite, rainfall amount is the dominant factor on

annual to decadal scales in eastern China (Li et al., 1998). Here we use rainfall record and Dry–Wet index record of Guiyang which have exactly age control to compare with the stalagmite δ18O (Fig. 9). The comparison shows that the δ18O was depleted during wet periods (marked by letter A, C, E, G in Fig. 9), and the δ18O became heavier during dry periods. It is clear that the δ18O records in Yelang Cave chiefly reflect wetness change, with lighter δ18O swing denoting a wet climatic condition; and vice versa.

5. Interpretation of δ18O and δ13C records of 20120824-13

5.1. Long-term climatic and vegetation variations since the last glaciation

Fig. 10 exhibits the δ18O and δ13C records of Stalagmite 20120824-13. Note that the section older than 13 kyr BP is plotted with depth rather than time. First of all, the Holocene δ18O trend of Stalagmite 20120824-13 is quite similar to that of Dongge Cave records (Yuan et al., 2004; Wang et al., 2005). This similarity demonstrates that the Holocene chronology of 20120824-13 record sounds good. Based on the δ18O and δ13C features, we can classify the climate and vegetation conditions of the studying area as following periods: (1) During MOIS 3 (below 140 mm), the δ18O and δ13C values were −10.6‰ to −9.2‰ and −7.7‰ to −4.3‰, respectively, indicating climatic condition was similar to the present, with moderate vegetation coverage. (2) During LGM (120–140 mm), the δ18O values were the heaviest, and the δ13C values were heavier than −4‰, reflecting very dry climates and poor vegetation coverage. The growth hiatus at this interval might be due to extremely arid climates. (3) During the Younger Dryas interval (12.5–11.5 kyr BP), the δ18O and δ13C values were also very heavy, representing dry climate and poor vegetation development. (4) During early Holocene (11.5–8 kyr BP), the δ18O decreased from 11.5 kyr BP to 9 kyr BP corresponding to the increased solar insolation. The δ18O values became the lightest in the entire record during the Holocene Optimum around 9 kyr BP, implying the strongest summer monsoon intensity under a maximum solar insolation. However, the δ13C values were not the lightest, and had a range similar to those in periods (1) and (5) (Fig. 10). It is a mystery that the stalagmite stopped to grow between 4.12 kyr BP and 8 kyr BP. This middle-to-late Holocene growth hiatus was found in four
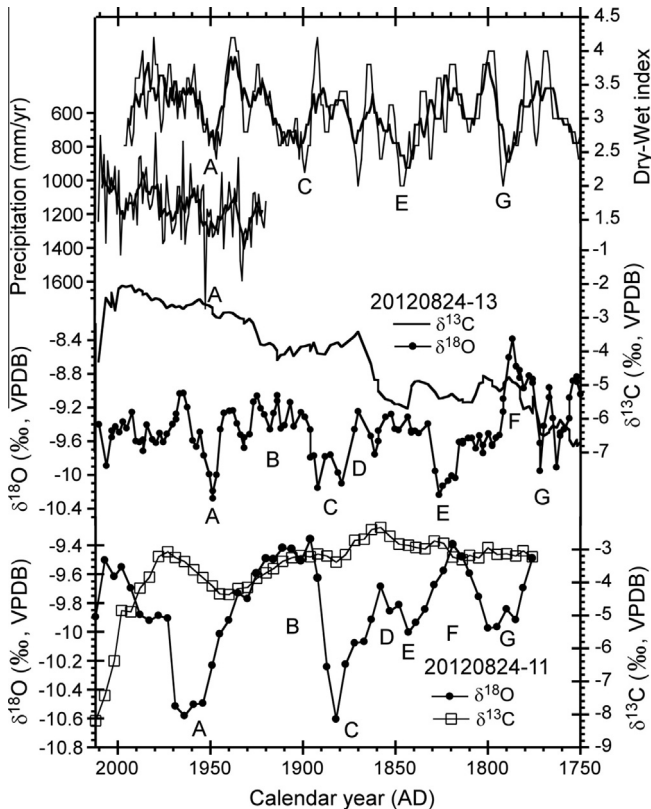

Fig. 9. Comparison of δ18O and δ13C records between 20120824-11 and -13, as well as their correlations with Guiyang rainfall record and Dry–Wet index record. The capital letters denote possible matching points among the δ18O records and rainfall record.
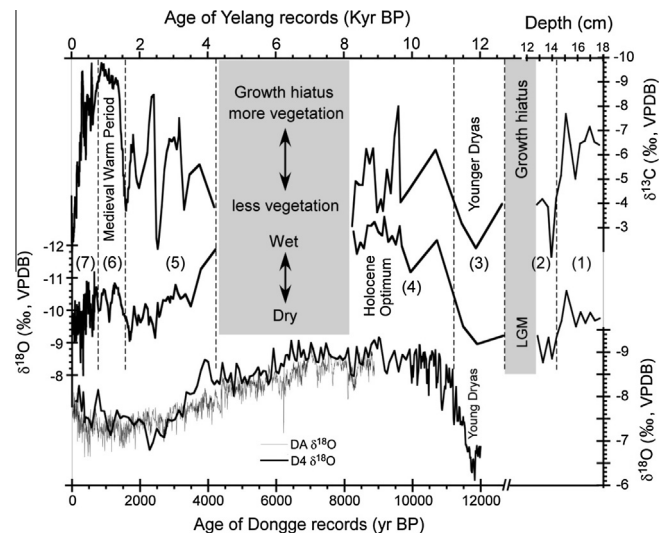

Fig. 10. The δ18O (upper) and δ13C (middle) records of Stalagmite 20120824-13 compared with the Dongge Cave δ18O records (lower), D4 (Yuan et al., 2004) and DA (Wang et al., 2005). Note that the X-axis of 20120824-13 record (top) changed to depth after 13,000 years BP, so that the two records are not the same on X-axes.

stalagmites from the same site in the cave. Normally, stalagmite grows fast under warm and wet conditions. The climatic conditions are expected warmer and wetter during 5–8 kyr BP than during late Holocene. Further investigation on an entire Holocene record from the cave is needed to uncover the mystery. (5) From 4.12 kyr BP to ~1.5 kyr BP, the stalagmite $\delta^{18}O$ had an increasing trend, denoting weakening summer monsoon strength during the late Holocene. This increasing trend also existed in the Dongge Cave records. The $\delta^{13}C$, on the other hand, did not appear an increasing trend. The fluctuations of the $\delta^{13}C$ record during this interval followed the $\delta^{18}O$ variation, showing that the vegetation development was sensitive to climatic changes. In addition, the large change of $\delta^{13}C$ values might reflect relatively thin soil coverage and vadose zone overlying the cave. (6) From ~1500 yr BP to ~600 yr BP, the $\delta^{18}O$ and $\delta^{13}C$ values were strongly depleted first from ~1500 yr BP to ~1200 yr BP, then remained relatively light. The $\delta^{13}C$ values were the lightest in the entire record, ranging −10 to −9‰. Both $\delta^{18}O$ and $\delta^{13}C$ records in this interval illustrate that the climate was wet and vegetation was abundant, perhaps corresponding to the Medieval Warm Period (Fig. 10). (7) During the past 600 yr BP, Stalagmite 20120824-13 record in this time period shows significant difference from the Dongge Cave records. The $\delta^{13}C$ was strongly increased, from −9‰ at ~600 yr BP to −2‰ around late 20th century, probably recording human impact on surface vegetation. The $\delta^{18}O$ of Stalagmite 20120824-13 had an increasing trend which was opposite to that of the Dongge Cave records. These opposite trends could not be caused by age error. On annual-to-centennial scales, climatic pattern has more spatial variations. It is not surprise to see the difference. If further evidence to support the difference, it is important for us to understand the discrepancy.

5.2. Climate change and human impact on vegetation during the past 600 years

The top 28 mm part of Stalagmite 20120824-13 has a fast growth rate and contains no growth hiatus (Fig. 6). Although the linear growth rate does not provide accurate chronology on annual-to-decadal scales, the general trends of the $\delta^{18}O$ and $\delta^{13}C$ records over the past 600 years should be reliable on multidecadal-to-centennial scales. A total of 328 samples of this part have been measured for $\delta^{18}O$ and $\delta^{13}C$, yielding records with about 2-yr resolution. Fig. 11 shows the comparisons of the $\delta^{18}O$ and $\delta^{13}C$ records of Stalagmite 20120824-13 ((a) and (b) in Fig. 11) with: (c) PDO index (Mantua et al., 1997; Shen et al., 2006), (d) Dry–Wet index of Guiyang, (e) Dry–Wet index of Eastern China (CAM, 1981; Zhang et al., 2003), (f) DA $\delta^{18}O$ record of Dongge Cave (Wang et al., 2005), (g) WX42B $\delta^{18}O$ record of Wanxiang Cave (Zhang et al., 2008), and (h) total solar irradiation (Delaygue and Bard, 2011). Among these records, (c), (d) and (e) have the same exactly calendar ages, and their chronologies are the most reliable. The longer PDO index record reconstructed by Shen et al. (2006) was actually based on the Dry–Wet index in East China. However, this record matches very well with the PDO index published by Mantua et al. (1997) (Fig. 11). These records are available on the NOAA website. The Dry–Wet index has clear physical meaning, so that the comparison begins from them. In order to understand the decadal variations, an 11-yr running average curve of the DWI records and the 500-yr PDO index record are used.

First of all, the Guiyang DWI record has similar variations with the E China DWI record during post-AD 1720. The later one represents average conditions of wetness change over the eastern China including three divisions: north China, south China and low-to-middle Yangtze River Drainage Basin. However, the two records are quite different prior to AD 1720, especially during AD
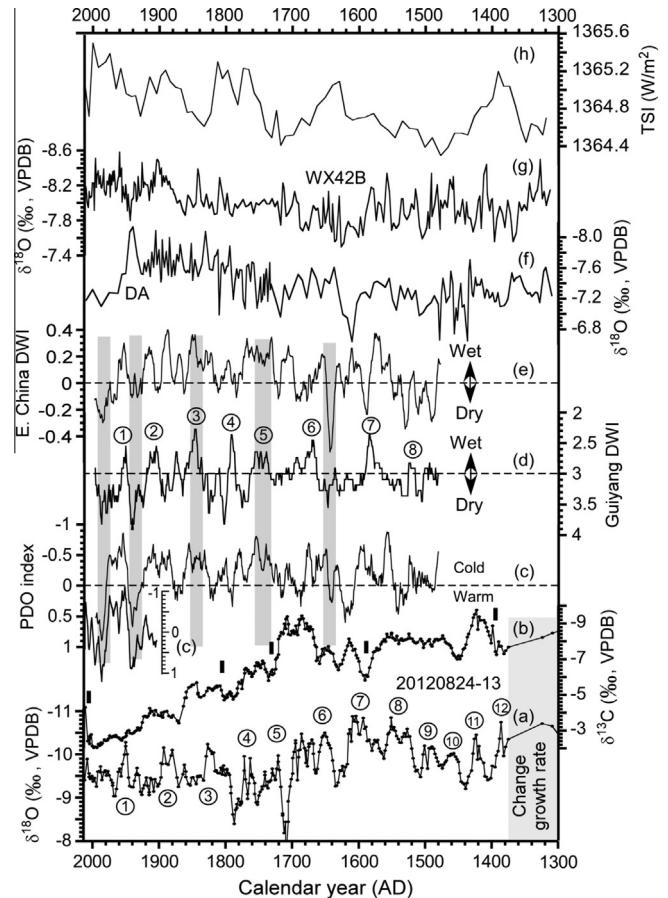

Fig. 11. The $\delta^{18}O$ and $\delta^{13}C$ records of 20120824-13 during the last 600 years, and their comparisons with (c) PDO index records (Mantua et al., 1997; Shen et al., 2006), (d) Dry–Wet index of Guiyang, (e) Dry–Wet index of Eastern China (Zhang et al., 2010), (f) the Dongge Cave $\delta^{18}O$ record (Wang et al., 2005), (g) the Wanxiang Cave $\delta^{18}O$ record (Zhang et al., 2008), and (h) Total solar irradiation (Delaygue and Bard, 2011). The block symbols near the $\delta^{13}C$ record denote the AMS ^{14}C dates locations. Numbers with circle represent wet periods.

1540-1660. This comparison indicates that spatial pattern may vary with climatic modes on decadal or shorter time scales. In Fig. 4, the comparisons of Guiyang rainfall and DWI with the PDO index have shown strong correlations. For the past 530 years, the Guiyang DWI record also compares well with the PDO index record, indicating that moisture condition of the studying area is strongly influenced by PDO condition on decadal scale. PDO is an ENSO-like pattern with a 20–30-yr long cycle in the Pacific. During cold phase of PDO like a La Niña condition, the eastern Pacific had a colder-than-normal sea surface temperature (SST) while the western and central North Pacific was warmer than normal (Fig. 4). The Walker Circulation shifted further west to bring more maritime moisture to Eastern China. The EASM could be stronger. The opposite situation occurs during a warm PDO phase which likes an El Niño condition.

The solar activity shown by the total solar irradiation does not exhibit clear correlation with the DWI records, perhaps having directly weak impact on the wetness condition of eastern China on decadal scales (Fig. 11). During higher solar irradiation periods of AD 1600-1640, 1720-1790, 1840-1890 and 1940-1970, the Guiyang and E China DWI records did not appear wetter than those in lower solar irradiation periods. Note that a very strong drought occurred around 1640 over eastern China. This was the years of Ming Dynasty collapse, ~40 years later than the weak monsoon period indicated by the WX42B $\delta^{18}O$ record. And, solar irradiation was high during this interval. Nevertheless, although changes in

solar activity will affect temperature and thermal contrast between land and ocean, this effect will be modified by oceanic and atmospheric circulations. Therefore, relationship between north Hemisphere temperature and the EASM strength is complicated on decadal or shorter time scales.

In fact, both the Wanxiang Cave and Dongge Cave $\delta^{18}O$ records which were claimed well-dated are difficult to compare with the DWI records of E China and Guiyang. Therefore, we do not anticipate that the $\delta^{18}O$ record of Stalagmite 20120824-13 can match the Guiyang DWI record. However, the 20120824-13 $\delta^{18}O$ record appears apparently decadal oscillations. At least 12 depleted $\delta^{18}O$ peaks (more than 0.5‰ change and longer than a decade) can be identified (Fig. 11). Eight of these peaks during the last 530 years might be corresponding to the wet periods shown in the Guiyang DWI record. In summary, the Yelang Cave $\delta^{18}O$ record reflects changes in wetness condition of the studying area on decadal scales, with lighter $\delta^{18}O$ corresponding to wet climates. The Pacific Decadal Oscillation is strongly affecting the wetness condition on decadal scales, with cold phase (La Niña state) in favor of wet climates in the studying area; and vice versa.

The $\delta^{13}C$ record of Stalagmite 20120824-13 mainly reflects vegetation change above the cave. During the last 600 years, the $\delta^{13}C$ ranged from −10‰ to −6‰ prior to AD 1720, but ranged from −7‰ to −2‰ post 1720. Before AD 1720, an increase in the $\delta^{13}C$ was following an increase of the $\delta^{18}O$, e.g., from AD 1420 to 1450, from 1560 to 1590, from 1620 to 1630, from 1700 to 1720 (Fig. 11). The increased $\delta^{13}C$ had sometimes several years of time lag with the $\delta^{18}O$, reflecting the responding duration of vegetation to climate change. Before AD 1720, when climate became wet shown by decreased $\delta^{18}O$, the $\delta^{13}C$ would decrease to values lighter than −7‰. However, the $\delta^{13}C$ had a continuously increasing trend after 1720. A wet climatic regime indicated by the strong depleted $\delta^{18}O$ peak from 1700 to 1720 did not cause the vegetation return to the previous status. Our hypothesis of the $\delta^{13}C$ anomaly after AD 1720 is the human impact on vegetation in the studying area. Deforestation in central Guizhou started from Ming Dynasty through military encampment and land cultivation (Han, 2006). However, large immigration toward west central Guizhou began the reign of Emperor Yong Zheng (AD 1722-1735) of Qing Dynasty due to mining of copper (Liang, 1980; Han, 2006). Historical records have documented that development of Guizhou peaked at the Yong Zheng-early Qianlong period of AD 1724-1753 when the extent and rapidity of population and land-use increase caused environmental deterioration. Since then, the vegetation coverage of the studying area has become worse. The damage of the natural vegetation caused by human activity led to soil loss and karst-desertification in central Guizhou. This karst-desertification was also recorded in Stalagmite ZJD-21 in Zhijin Cave (Kuo et al., 2011). Interestingly, the $\delta^{13}C$ values of the surface sample in Stalagmite 20120824-13 and several top samples in 20120824-11 became significantly lighter, probably reflecting the vegetation recovery made by recent management of karst-desertification mitigation. The fact that 20120824-13 $\delta^{13}C$ record agrees with the historic documents manifests reliability of the stalagmite record. In addition, the four AMS ^{14}C dates that have significant dead carbon influence during this interval are all located in the heavier $\delta^{13}C$ periods. The AMS ^{14}C date at 1400 yr BP which has negligible dead carbon influence shows light $\delta^{13}C$ value. Poor vegetation coverage leads to less contribution of organic carbon and more dead carbon fraction.

6. Conclusions

We use ICPMS ^{230}Th/U, ^{210}Pb and AMS ^{14}C dating methods to build up the chronology of the stalagmites from Yelang Cave in

central Guizhou of China. Low U content and relatively high Th content in the stalagmites cannot provide reliable ^{230}Th/U dates for chronological reconstruction. The AMS ^{14}C dates, on the other hand, exhibit small dating uncertainties and better age sequences. Based on the AMS ^{14}C dates, we have established the chronology of the stalagmites which is supported by the comparisons of the stalagmite record with the instrumental and historic climate records. When vegetation intensity above the cave decreases, the stalagmite $\delta^{13}C$ becomes heavier and the DCF in the stalagmite increases. Intensively detailed AMS ^{14}C dating on a stalagmite that has low U but high Th contents can produce ^{14}C ages with minimal dead carbon influence. With these reliable ^{14}C ages, the chronology of the stalagmite that is not able to be dated by ICPMS ^{230}Th/U can be established. In addition, the initial ^{230}Th correction of ^{230}Th/U age for such a low U, high Th and young sample will be problematic.

Based on the growth features, $\delta^{18}O$ and $\delta^{13}C$ records of Stalagmite 20120824-13, we have reconstructed climate and vegetation changes in the studying area since 50 kyr BP: (1) climatic condition during MOIS 3 was similar to the present with moderate vegetation coverage. (2) Very dry climates and poor vegetation coverage existed during the LGM and the Younger Dryas interval. (3) Increased precipitation and vegetation coverage occurred during early Holocene, corresponding to the increased solar insolation. The strongest summer monsoon intensity over Holocene presented during the Holocene Optimum around 9 kyr BP under a maximum solar insolation. However, it is unknown that the stalagmite did not grow during the Bølling–Allerød interval (13–15 kyr BP) and between 4.12 and 8 kyr BP. (4) The EASM strength started to decrease from the beginning of late Holocene corresponding to the decreased solar insolation. (5) Wet climate and good vegetation coverage were prevailing during the Medieval Warm Period. (6) High-resolution $\delta^{18}O$ record during the last 600 years exhibits strong decadal climate changes. Comparisons among the $\delta^{18}O$ records, DWI, PDO index and solar irradiation illustrate that PDO strongly affects decadal variability of the moisture budget in the studying area, with cold PDO (La Niña condition) in favor of stronger EASM and wet climates. The natural vegetation in the studying area was strongly destroyed by human activity after the reign of Emperor Yong Zheng (AD 1722-1735) of Qing Dynasty. Since then, the karst-desertification in central Guizhou has been strongly developed due to rapidly increased population and land-use.

References

Allan, R.J., Nicholls, N., Jones, P.D., Butterworth, I.J., 1991. A further extension of the Tahiti-Darwin SOI, early SOI results and Darwin pressure. J. Clim. 4, 743–749.

Baker, A., Ito, E., Smart, P.L., McEwan, R.F., 1997. Elevated and variable values of ^{13}C in speleothems in a British cave system. Chem. Geol. 136, 263–270.

Bar-Matthews, M., Ayalon, A., Matthews, A., Sass, E., Halicz, L., 1996. Carbon and oxygen isotope study of the active water carbonate system in a karstic Mediterranean cave: implications for paleoclimate research in semiarid regions. Geochim. Cosmochim. Acta 60, 337–347.

Beck, J.W., Richards, D.A., Edwards, R.L., Silverman, B.W., Smart, P.L., Donahue, D.J., Hererra-Osterheld, S., Burr, G.S., Calsoyas, L., Jull, A.J.T., Biddulph, D., 2001. Extremely large variations in atmospheric C-14 concentration during the last glacial period. Science 292, 2453–2458.

Cheng, H., Edwards, R.L., Shen, C.-C., Polyak, V.J., Asmerom, Y., Woodhead, J., Hellstrom, J., Wang, Y.J., Kong, X.G., Spötl, C., Wang, X.F., Alexander Jr., E.C., 2013. Improvements in ^{230}Th dating, ^{230}Th and ^{234}U half-life values, and U–Th isotopic measurements by multi-collector inductively coupled plasma mass spectrometry. Earth Planet. Sci. Lett. 371–372, 82–91.

Chinese Academy of Meteorological Sciences (CAM), 1981. Yearly Charts of Dryness/Wetness in China for the Last 500-Year Period, Beijing. SinoMap, Beijing (in Chinese).

Chu, P.-C., Li, H.-C., Fan, C.-W., Chen, Y.-H., 2012. Speleothem evidence for temporal-spatial variation in East Asian Summer monsoon since Medieval Warm period. J. Quat. Sci. 27 (9), 901–910.

Cosford, J., Qing, H.R., Mattey, D., Eglington, B., Zhang, M.L., 2009. Climatic and local effects on Stalagmites $\delta^{13}C$ values at Lianhua Cave, China. Paleogeogr., Paleoclimatol., Paleoecol. 280, 235–244.

Denniston, R.F., Wyrwoll, K.H., Polyak, V.J., Brown, J.R., Asmerom, Y., Wanamaker Jr., A.D., LaPointe, P., Ellerbroek, R., Barthelmes, M., Cleary, D., Cugley, J., Woods, D., Humphreys, W.F., 2013. Stalagmite record of Holocene Indonesian –Australian summer monsoon variability from the Australian tropics. Quatern. Sci. Rev. 78, 155–168.

Delaygue, G., Bard, E., 2011. An antarctic view of Beryllium-10 and solar activity for the past millennium. Clim. Dyn. 36, 2201–2218.

Dorale, J.A., Gonzálex, L.A., Reagan, M.K., Pickett, D.A., Murrell, M.T., Baker, R.G., 1992. A high-resolution record of Holocene climate change in speleothem calcite from cold water cave, Northeast Iowa. Science 258, 1626–1630.

Dykoski, C.A., Edwards, R.L., Cheng, H., Yuan, D.X., Cai, Y.J., Zhang, M.L., Lin, Y.S., Qing, J.M., An, Z.S., Revenaugh, J., 2005. A high-resolution, absolute-dated Holocene and deglacial Asian monsoon record from Dongge Cave, China. Earth Planet. Sci. Lett. 233, 71–86.

Fairchild, I., Smith, C.L., Baker, A., Fuller, L., Spötl, C., Mattey, D., McDermott, D.E.I.M.F., 2006. Modification and preservation of environmental signals in speleothems. Earth Sci. Rev. 75, 105–153.

Fleitmann, D., Cheng, H., Badertscher, B., Edwards, R.L., Mudelsee, M., Göktürk, O.M., Fankauser, A., Pickering, R., Raible, C.C., Matter, A., Kramers, J., Tüysüz, O., 2009. Timing and climatic impact of Greenland interstadials recorded in stalagmites from northern Turkey. Geophys. Res. Lett. 36 (19), L17909. http://dx.doi.org/10.1029/2009GL040050.

Friedman, I., O'Neil, J.R., 1977. Compilation of Stable Isotope Fractionation Factors of Geochemical Interest. US Geological Survey Professional Paper, P-0440-KK, pp. 1–12.

Genty, D., Baker, A., Massault, M., Proctor, C., Gilmour, M., Pons-Branchu, E., Hamelin, B., 2001. Dead carbon in stalagmites: carbonate bedrock paleodissolution vs. ageing of soil organic matter. Implications for ^{13}C variations in speleothems. Geochim. Cosmochim. Acta 65, 3443–3457.

Genty, D., Blamart, D., Ouahdi, R., Gilmour, M., Baker, A., Jouzel, J., Van-Exter, S., 2003. Precise dating of Dansgaard–Oeschger climate oscillations in western Europe from stalagmite data. Nature 421, 833–837.

Genty, D., Blamart, D., Ghaleb, B., Plagnes, V., Causse, Ch., Bakalowicz, M., Zouari, K., Chkir, N., Hellstrom, J., Wainer, K., Bourge, F., 2006. Timing and dynamics of the last deglaciation from European and North African $\delta^{13}C$ stalagmite profiles-comparison with Chinese and South Hemisphere stalagmites. Quatern. Sci. Rev. 25, 2118–2142.

Genty, D., Combourieu-Nebout, N., Peyron, O., Blamart, D., Wainer, K., Mansuri, F., Ghaleb, B., Isabello, L., Dormoy, I., Grafenstein, U., Bonelli, S., Landais, A., Brauer, A., 2010. Isotopic characterization of rapid climatic events during OIS3 and OIS4 in Villars Cave stalagmites (SW-France) and correlation with Atlantic and Mediterranean pollen records. Quatern. Sci. Rev. 29, 2799–2820.

Han, Z.Q., 2006. Exploitation of Guizhou province during the Yongzheng reign period and its effect on the rock-desertification in this area. Fudan J. (Soc. Sci.) 2, 120–140 (in Chinese).

Hendy, C.H., 1971. The isotopic geochemistry of speleothems—I. The calculation of the effects of different modes of formation on the isotopic composition of speleothems and their applicability as paleoclimate indicators. Geochim. Cosmochim. Acta 35, 801–824.

Hiess, J., Condon, D.J., McLean, N., Noble, S.R., 2012. $^{238}U/^{235}U$ systematics in terrestrial U-bearing minerals. Science 335 (6076), 1610–1614.

Hoffmann, D.L., Beck, J.W., Richards, D.A., Smart, P.L., Singarayer, J.S., Ketchmark, T., Hawkesworth, C.J., 2010. Towards radiocarbon calibration beyond 28 ka using speleothems from the Bahamas. Earth Planet. Sci. Lett. 289, 1–10.

Hu, C.Y., Henderson, G.M., Huang, J., Xie, S.C., Sun, Y., Johnson, K.R., 2008. Quantification of Holocene Asian monsoon rainfall from spatially separated cave records. Earth Planet. Sci. Lett. 266, 221–232.

IPCC, 2007. Climate Change 2007 – The physical science basis. In: Solomon, S., Qin, D., Manning, M., Chen, Z., Marquis, M., Averyt, K.B., Tignor, M., Miller, H.L. (Eds.), Contribution of Working Group I to the Fourth Assessment Report of the Intergovernmental Panel on Climate Change. Cambridge University Press, Cambridge, United Kingdom and New York, NY, USA, p. 996.

Jaffey, A.H., Flynn, K.F., Glendenin, L.E., Bentley, W.C., Essling, A.M., 1971. Precision measurement of half-lives and specific activities of ^{235}U and ^{238}U. Phys. Rev. C 4, 1889–1906.

Kotlia, B.S., Ahmad, S.M., Zhao, J.X., Raza, W., Collerson, K.D., Joshi, L.M., Sanwal, J., 2012. Climatic fluctuations during the LIA and post-LIA in the Kumaun Lesser Himalaya, India: evidence from a 400 y old stalagmite record. Quatern. Int. 263 (14), 129–138.

Ku, T.-L., Li, H.-C., 1998. Speleothems as high-resolution paleoenvironment archives: records from northeastern China. J. Earth Syst. Sci. 107, 321–330.

Kuo, T.-S., Liu, Z.-Q., Li, H.-C., Wan, N.-J., Shen, C.-C., Ku, T.-L., 2011. Climate and environmental changes during the past millennium in central western Guizhou reflected by Stalagmite ZJD-21 record. J. Asian Earth Sci. 40, 1111–1120.

Li, H.-C., Ku, T.L., Chen, W.-J., Jiao, W.Q., Zhao, S.S., Chen, T.M., Li, T.Y., 1996. Isotope studies of Shihua Cave, Beijing —II: radiocarbon dating and age correction of stalagmite. Seismol. Geol. 18, 329–338.

Li, H.-C., Ku, T.-L., Stott, L.D., Chen, W.J., 1998. Applications of interannual-resolution stable isotope records of speleothem: climatic changes in Beijing and Tianjin, China during the past 500 years — the $\delta^{18}O$ record. Sci. China 41, 362–368.

Li, H.-C., Lee, Z.-H., Wan, N.-J., Shen, C.-C., Li, T.Y., Yuan, D.X., Chen, Y.H., 2011a. Interpretations of $\delta^{18}O$ and $\delta^{13}C$ in aragonite stalagmites from Furong Cave, Chongqing, China: A 2000-year record of monsoonal climate. J. Asia Earth Sci. 40, 1121–1130.

Li, T.-Y., Shen, C.-C., Li, H.-C., Li, J.-J., Chiang, H.-W., Song, S.-R., Yuan, D.-X., Lin, Chris D.-J., Gao, P., Zhou, L.-P., Wang, J.-L., Ye, M.-Y., Tang, L.-L., 2011b. Oxygen and carbon isotopic systematics of aragonite speleothems and water in Furong Cave, Chongqing, China. Geochim. Cosmochim. Acta 75, 4140–4156.

Li, T.-Y., Li, H.-C., Xiang, X.-J., Kuo, T.-S., Li, J.-Y., Zhou, F.-L., Chen, H.-L., Peng, L.-L., 2012. Transportation characteristics of $\delta^{13}C$ in the plants-soil-bedrock -cave system in Chongqing karst area. Sci. China (D) 55, 685–694. http://dx.doi.org/10.1007/s11430-011-4294-y.

Liang, F.Z., 1980. The Statistics of Family Numbers, Farmland Areas, Farm Taxes in Chinese History. Shanghai People Press, p. 272 and p. 380 (in Chinese).

Linge, H., Lauritzen, S.E., Lundberg, J., Berstad, I.M., 2001. Stable isotope stratigraphy of Holocene speleothems: examples from a cave system in Rana, northern Norway. Paleogeogr., Paleoclimatol., Paleoecol. 167, 209–224.

Mantua, N.J., Hare, S.R., Zhang, Y., Wallace, J.M., Francis, R.C., 1997. A Pacific interdecadal climate oscillation with impacts on salmon production. Bull. Am. Meteorol. Soc. 78, 1069–1079.

O'Neil, J.R., Clayton, R.N., Mayeda, T.K., 1969. Oxygen isotope fractionation in divalent metal carbonates. J. Chem. Phys. 51, 5547–5558.

Oster, J.L., Montañez, I.P., Guilderson, T.P., Sharp, W.D., Banner, J.L., 2010. Modeling speleothem $\delta^{13}C$ variability in a central Sierra Nevada cave using ^{14}C and $^{87}Sr/^{86}Sr$. Geochim. Cosmochim. Acta 74, 5228–5242.

Oster, J.L., Montañez, I.P., Kelley, N.P., 2012. Response of a modern cave system to large seasonal precipitation variability. Geochim. Cosmochim. Acta 91, 92–108.

Paulsen, D.E., Li, H.-C., Ku, T.-L., 2003. Climate variability in central China over the last 1270 years revealed by high-resolution stalagmite records. Quatern. Sci. Rev. 22, 691–701.

Pausata, F.S.R., Battisti, D.S., Nisancioglu, K.H., Bitz, C.M., 2011. Chinese stalagmite $\delta^{18}O$ controlled by changes in the Indian monsoon during a simulated Heinrich event. Nature 4, 474–480.

Shen, C.-C., Edwards, R.L., Cheng, H., Dorale, J.A., Thomas, R.B., Moran, S.B., Weinstein, S.E., 2002. Uranium and thorium isotopic and concentration measurements by magnetic sector inductively coupled plasma mass spectrometry. Chem. Geol. 185, 165–178.

Shen, C.-C., Cheng, H., Edwards, R.L., Moran, S.B., Edmonds, H.N., Hoff, J.A., Thomas, R.B., 2003. Measurement of attogram quantities of ^{231}Pa in dissolved and particulate fractions of seawater by isotope dilution thermal ionization mass spectroscopy. Anal. Chem. 75, 1075–1079.

Shen, C.-C., Wu, C.-C., Cheng, H., Edwards, R.L., Hsieh, Y.-T., Gallet, S., Chang, C.-C., Li, T.-Y., Lam, D.D., Kano, A., Hori, M., Spötl, C., 2012. High-precision and high-resolution carbonate ^{230}Th dating by MC-ICP-MS with SEM protocols. Geochim. Cosmochim. Acta 99, 71–86.

Shen, C.M., Wei-Chyung Wang, W.-C., Gong, W., Hao, Z.X., 2006. A Pacific Decadal Oscillation record since 1470 AD reconstructed from proxy data of summer rainfall over eastern China. Geophys. Res. Lett. 33, L03702. http://dx.doi.org/10.1029/2005GL024804.

Southon, J., Noronha, A.L., Cheng, H., Edwards, R.L., Wang, Y.J., 2012. A high-resolution record of atmospheric ^{14}C based on Hulu Cave speleothem H82. Quatern. Sci. Rev. 33, 32–41.

Stuiver, M., Reimer, P.J., 1986. A computer program for radiocarbon age calibration. Radiocarbon 28 (2B), 1022–1030.

Stuiver, M., Reimer, P.J., 1993. Extended ^{14}C data base and revised CALIB 3.014 C age calibration program. Radiocarbon 35, 215–230.

Wan, N.-J., Chung, W.-L., Li, H.-C., Lin, H.L., Shen, C.-C., Ku, T.-L., Yuan, D.X., Zhang, M.L., Lin, Y.S., 2011a. The comparison of speleothem $\delta^{18}O$ records from Eastern China with solar insolation, ice core and marine records: similarities and discrepancies on different time scales. J. Asia Earth Sci. 40, 1151–1163.

Wan, N.-J., Li, H.-C., Liu, Z.Q., Yuan, D.X., 2011b. Spatial variations of monsoonal rain in eastern China: instrumental, historic and speleothem records. J. Asia Earth Sci. 40, 1139–1150.

Wang, X.F., Auler, A.S., Edwards, L.R., Cheng, H., Ito, E., Solheid, M., 2006. Interhemispheric anti-phasing of rainfall during the last glacial period. Quatern. Sci. Rev. 25, 3391–3403.

Wang, Y.J., Cheng, H., Edwards, R.L., An, Z.S., Wu, J.Y., Shen, C.-C., Dorale, J.A., 2001. A high-resolution absolute-dated late Pleistocene monsoon record from Hulu Cave, China. Science 294, 2345–2348.

Wang, Y.J., Cheng, H., Edwards, R.L., He, Y., Kong, X., An, Z.S., Wu, J., Kelly, M.J., Dykoski, C.A., Li, X., 2005. The Holocene Asian monsoon: links to solar changes and north Atlantic climate. Science 308, 854–857.

Wang, Y.J., Cheng, H., Edwards, R.L., Kong, X., Shao, X., Chen, S., Wu, J., Jiang, X., Wang, X., An, Z.S., 2008. Millennial- and orbital-scale changes in the East Asian monsoon over the past 224,000 years. Nature 451, 1090–1093.

Yang, Y., Yuan, D.X., Cheng, H., Zhang, M.L., Qin, J.M., Lin, Y.S., Zhu, X.Y., Edwards, L.R., 2010. Precise dating of abrupt shifts in the Asian Monsoon during the last deglaciation based on stalagmite data from Yamen Cave, Guizhou Province, China. Earth Sci. 53 (5), 633–641.

Yin, J.J., Yuan, D.X., Li, H.-C., Cheng, H., Li, T.Y., Edwards, R.L., Lin, Y.S., Qin, J.M., Tang, W., Zhao, Z.Y., Mii, H.S., 2014. Variation in the Asian monsoon intensity and dry–wet condition since the Little Ice Age in central China revealed by an

aragonite stalagmite. Clim. Past 10, 1803–1816. http://dx.doi.org/10.5194/cp-10-1803-2014.

Yuan, D.X., Cheng, H., Edwards, R.L., Dykoski, C.A., Kelly, M.J., Zhang, M.L., Qing, J.M., Lin, Y.S., Wang, Y.J., Wu, J., Dorale, J.A., An, Z.S., Cai, Y.J., 2004. Timing, duration, and transition of the last interglacial Asian monsoon. Science 304, 575–578.

Zhang, M.L., Yuan, D.X., Lin, Y.S., Qin, J.M., Bin, L., Cheng, H., Edwards, R.L., 2004. A 6000-year high-resolution climatic record from a stalagmite in Xiangshui Cave, Guilin, China. The Holocene 14 (5), 697–702.

Zhang, M.-L., Zhu, X.-Y., Lin, Y.-S., Cheng, K.-K., He, S.-Y., Wang, H., Yang, Y., 2009. Cave dripping water and carbon isotopic records of modern carbonate(CaCO3)deposits: stalagmite in Panlong Cave of Guilin and its environmental significance. Acta Geoscientica Sin. 30 (5), 634–642.

Zhang, D.E., Li, H.-C., Ku, T.-L., Lu, L.H., 2010. On linking climate to Chinese dynastic change: spatial and temporal variations of monsoonal rain. Chin. Sci. Bull. 55, 77–83.

Zhang, D.E., Li, X.Q., Liang, Y.Y., 2003. Continuation (1992–2000) of the yearly charts of dryness/wetness in China for the last 500 years period. J. Appl. Meteorol. Sci. 14, 379–388 (in Chinese with English abstract).

Zhang, H.-L., Yu, K.-F., Zhao, J.-X., Feng, Y.-X., Lin, Y.-S., Zhou, W., Liu, G.-H., 2013. East Asian summer monsoon variations in the past 12.5 ka: high-resolution $\delta^{18}O$ record from a precisely dated aragonite stalagmite in central China. J. Asian Earth Sci. 73, 162–175.

Zhang, P.Z., Cheng, H., Edwards, R.L., Chen, F.H., Wang, Y.J., Yang, X.L., Liu, J., Tan, M., Wang, X.F., Liu, J.H., An, C.L., Dai, Z.B., Zhou, J., Zhang, D.Z., Jia, J.H., Jin, L.Y., Johnson, K.R., 2008. A test of climate, sun, and culture relationships from an 1810-year Chinese cave record. Science 322, 940–942.

Zhu, X.Y., Zhang, M.L., Lin, Y.S., Qin, J.M., Yang, Y., 2006. Carbon isotopic records from stalagmites and the signification of paleo-ecological environment in the area of Guangxi—Guizhou, China. Environ. Geol. 51, 267–273.